Aerosol and Air Quality Research, 17: 1011–1020, 2017

ISSN: 1680-8584 print / 2071-1409 online
doi: 10.4209/aaqr.2017.01.0013

Effect of MnO_2 Crystalline Structure on the Catalytic Oxidation of Formaldehyde

Huiqi Lin, Dong Chen*, Haibo Liu, Xuehua Zou, Tianhu Chen**

Laboratory for Nanomineralogy and Environmental Material, School of Resources and Environmental Engineering, Hefei University of Technology, Hefei 230009, China

ABSTRACT

Manganese oxides prove to be a promising catalyst for formaldehyde (HCHO) elimination in catalytic oxidation. In this study, MnO_2 with different crystalline structure (α-MnO_2, β-MnO_2, γ-MnO_2, and δ-MnO_2) were synthesized by hydrothermal method to investigate their catalytic performances towards the abatement of formaldehyde. The prepared catalysts were characterized and analyzed by the X-ray diffraction (XRD), hydrogen-temperature programmed reduction (H_2-TPR), BET specific surface area, X-ray photoelectron spectroscopy (XPS), and ammonia-temperature programmed desorption (NH_3-TPD). In addition, the apparent activation energy was also calculated by using Arrhenius plots. Among the above four prepared catalysts, the γ-MnO_2 has the best destruction and removal efficiency (DRE), which was approaching to 100% for HCHO at 155°C. The catalytic activity of γ-MnO_2 is associated with abundant mesopores, higher reducibility of surface oxygen species, and more oxygen vacancies as compared to other types of crystalline MnO_2.

Keywords: MnO_2; Catalytic oxidation; Formaldehyde; Surface oxygen; Temperature programmed reduction.

INTRODUCTION

Formaldehyde (HCHO), one of typical Volatile organic compounds (VOCs), is considered to be the major pollutant in indoor air (Wang and Li, 2010; Wu *et al.*, 2015a; Zeng and Bai, 2016). However, HCHO has been widely used in the industrial production, such as plastic, rubber, resin, adhesives and plywood. Ii is easily emitted into the air from the production and consumption from the relevant products, resulting in many healthy and environmental issues. In addition, the indoor formaldehyde is mainly derived from the burning of cigarettes, as well as a variety of decorative materials (Kim, 2009; Tang *et al.*, 2009; Wu *et al.*, 2015b). According to the reports, people who engaged in formaldehyde related occupations are more likely to have cancer, and the incidence of eye and respiratory irritation symptoms will be significantly increased as well (Collins *et al.*, 2001; Silbergeld and Patrick, 2005).

At present, the removal methods of formaldehyde in the air mainly include adsorption, photocatalytic oxidation, thermal catalytic oxidation and so on (Spivey, 1987; Atkinson and Arey, 2003a; b; Zhou *et al.*, 2011; Ewlad-Ahmed *et al.*, 2012; Yu *et al.*, 2015; Bai *et al.*, 2016; Hosseini *et al.*, 2016; Liang *et al.*, 2016; Liu *et al.*, 2016; Yu *et al.*, 2016). High specific surface materials, such as activated carbon and molecular sieve are common used in adsorption technology to remove formaldehyde (Kosuge *et al.*, 2007; Ma *et al.*, 2011; Chen *et al.*, 2014), but the difficulty of regeneration on absorbent have restricted the applicant in high concentration of HCHO. At room temperature, HCHO can be decomposed through the activity of hydroxyl radicals and superoxide radicals by using TiO_2 nanoparticles as photocatalyst. In photocatalytic oxidation, the requirement of UV excitation light source reduces the application of visible light in the environment. Moreover, the deactivation of catalyst is another restrictive factor for photocatalytic oxidation. Due to the advantage of its high removal efficiency, low cost, no secondary pollution, the thermal catalytic oxidation has been extensively used in the HCHO abatement. The catalyst can be classified to the supported noble metal catalyst (Au/ZrO_2, Ag/Al_2O_3, Pd/TiO_2 and Pt/Fe_2O_3) and transition metal oxide (CeO_2, MnO_x and Co_3O_4) (Zhou *et al.*, 2011; Chen *et al.*, 2014, 2015; Bai *et al.*, 2016; Hosseini *et al.*, 2016). Among them, manganese oxide catalysts showed excellent performance, even better than supported noble metal catalysts in the low temperature environment.

Among transition metal oxide materials, MnO_2 has an extremely rich structure and morphology. There are α-MnO_2, β-MnO_2, γ-MnO_2 and other forms, which has the same structure unit: MnO_6 octahedra, the oxygen atom is located on the top of the eight surface body angle, while

* Corresponding author.
Tel.: +86- 139-5517-6245
E-mail address: cdxman@hfut.edu.cn
** Corresponding author.
Tel.: +86-551-6290-3990
E-mail address: chentianhu@hfut.edu.cn

the manganese atom is in the center of the eight surface body. The valence shell electron configuration of the metal manganese is $3d^5 4s^2$, which means five electrons in the D orbit are in the unsaturated state, and this will result in the electronic gain-and-loss easier to occur, as well as strong oxidation reduction performance. In the process of catalysis, the gain and loss of the electron is the key for the formation of active intermediates (Wang *et al.*, 2015).

In this study, four different types of MnO_2 crystal structures were prepared and then, their properties, performance and reaction mechanism of the formaldehyde catalytic oxidation were investigated and discussed.

EXPERIMENTAL

Preparation of Catalysts

The catalysts were prepared by hydrothermal method. In a typical synthesis of the α-MnO_2 catalysts, 1.05 g $MnSO_4 \cdot H_2O$ and 2.50g $KMnO_4$ were mixed in the distilled water (160 mL) and adding 4mL concentrated HNO_3, then magnetically stirred about 1 h to form a homogeneous mixture. After stirring, the mixture was transferred into a Teflon reactor (200 mL) and heated at 100°C for 24 h. Similarly, the δ-MnO_2 were obtained from the reaction of $KMnO_4$ (3.0 g) and $MnSO_4.H_2O$ (0.55 g) at 240°C for 24 h. For the preparation of the β-MnO_2, $(NH_4)_2S_2O_8$ (4.56 g) and $MnSO_4 \cdot H_2O$ (3.38 g) were well mixed and hydrothermally treated at 140°C for 12 h. The products of the above reaction were collected and centrifugal washed for 3–5 times, then dried at 100°C overnight, the obtained solid sample was calcinated at 400°C for 2 h, then ground to 40–60 mesh standby (Yuan *et al.*, 2003; Jin *et al.*, 2009;). For γ-MnO_2, 0.06 mol L^{-1} $KMnO_4$ solution and 0.08 mol L^{-1} $MnSO_4$ solution (the mixed ratio is 5:6, respectively) were mixed and transferred into 1 L beaker under vigorous stirring for 30 min. Then the mixed solution was further aged for 30 min. After that, the precipitation was collected by filtration using buchner funnel, and washed by deionized water until there is no SO_4^{2-} in filtrate (test with 0.2 mol L^{-1} barium chloride solution). The precipitation is dried at 80°C, crushing to obtain γ-MnO_2 (Jin *et al.*, 2009).

Characterization

XRD analysis was performed using a D/max-RB type X ray diffraction instrument, with a Cu radiation source, at a scanning speed of 4° min^{-1}, 50 kV tube voltage, and 30 mA tube current, the scanning range is 5°–70°. The specific area (BET) analyses of the sample were investigated using a Quantachrome NOVA 3000e analyzer at –196°C. The pore size distribution was calculated by the desorption branch of the N_2 adsorption-desorption isotherm using the BJH method. Before the N_2 physisorption, the catalysts were degassed at 300°C for 5 h. H_2-TPR test was carried out in a micro reactor from room temperature up to 600°C under 5% H_2/Ar mixture atmosphere over 50 mg catalyst, gas velocity is 30 mL min^{-1} and heating rate is 10 °C min^{-1}. For NH_3-TPD analysis, 100 mg catalyst was taken in a tubular fixed bed flow reactor of quartz (i.d. = 6 mm). heated to 300°C and then swept with Ar for 1 h. After natural cooling to 100°C, the catalyst was purged with 0.05% NH_3/Ar for about 100 min. Until the adsorption ended, NH_3 desorption was carried out from 100°C to 450°C at a heating rate of 10 °C min^{-1} in Ar atmosphere, and then the temperature was maintained at 450°C for 1h to ensure complete desorption of samples. A mass spectrometer (Hiden QIC-20) was used as a gas detector in the outlet gas.

Catalytic Activity Test

The quartz tube of 6 mm id is used as a fixed bed reactor while experimental temperature ranges from 100°C to 350°C. 60 mg catalyst placed in the reactor is heated by a tubular furnace at a heating rate of 10 °C min^{-1}. The feed gas composition was 1400 ppm HCHO balanced by the air. The high concentration of HCHO used in this study was to simulate the normal condition of industrial formaldehyde. Gaseous HCHO was produced by flowing dry air over the paraformaldehyde at 38°C. Before the air flow through the reactor, all dry air was purged by sodium hydroxide pellet to clean out residual CO_2 and H_2O. The gas velocity was 100 mL min^{-1}. The removal rate of HCHO was calculated by the yield of CO_2.

$$CO_2 = \frac{C_{CO_2}}{C^*_{CO_2}} \times 100\% \quad (1)$$

where C^*_{CO2} is the CO_2 concentration in the outlet gas when HCHO oxidized completely and C_{CO2} is that at different temperatures. The concentration of CO_2 in the effluent was recorded by a Jena Analytik multi N/C 2100 TOC analyzer (Liu *et al.*, 2013).

RESULTS AND DISCUSSION

Physical Properties and Crystal Structure of Catalysts

XRD patterns were measured to investigate the crystallographic structures of the samples and the results are shown in Fig. 1. Fig. 1(a) shows the characteristic diffraction peaks at 2θ = 12.7, 18.0, 25.5, 37.4, 41.8, 52.0, 55.3 and 60.0°, which corresponding to tetragonal α-MnO_2. The sharp diffraction peaks in Fig. 1(b) at 2θ = 28.5, 37.3, 41.0, 42.8 and 56.6° can be attributed to β-MnO_2. Similarly, Fig. 1(c) displays the crystal plane diffraction peak of δ-MnO_2 at 2θ = 12.2, 25.0 and 37.3°. Fig. 1(d) represents the diffraction peaks at 2θ = 22.1, 37.0, 42.0 and 56.7°, respectively, this is consistent with XRD pattern of γ-MnO_2. It's not hard to find that the characteristic diffraction peak intensity of γ-MnO_2 and δ-MnO_2 is obviously weaker than that of α-MnO_2 and β-MnO_2, which indicates the low crystallinity of these two catalysts.

Specific surface area is used to characterize the adsorption properties and activity of porous materials. Table 1 shows the specific surface area (BET), total pore volume (Vp) and average pore size (Dp) of the catalyst samples. It turns out that there are big differences between the specific surface area of MnO_2 catalysts with diverse crystal type, and the average pore size variation law is α-MnO_2 > β-MnO_2 > δ-MnO_2 > γ-MnO_2, while the change law of the total pore volume is

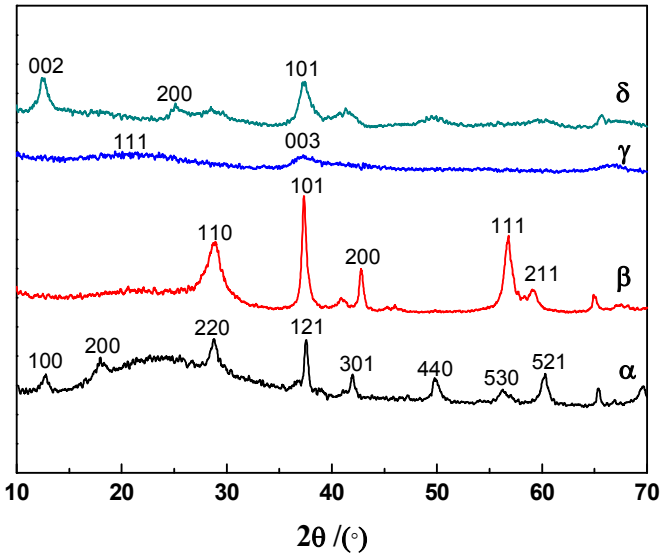

Fig. 1. XRD patterns of (a) α-MnO_2, (b) β-MnO_2, (c) γ-MnO_2, and (d) δ-MnO_2.

Table 1. BET results of MnO_2 catalysts with different crystal phases.

Manganese oxides	S_{BET}/(m^2 g^{-1})	V_P/(cc g^{-1})	D_P/(nm)
α-MnO_2	44.60	0.215	19.5
β-MnO_2	24.17	0.081	13.3
γ- MnO_2	96.97	0.116	4.6
δ- MnO_2	109.21	0.349	12.8

δ-MnO_2 > α-MnO_2 > γ-MnO_2 > β-MnO_2, specific surface area variation law is δ-MnO_2 > γ-MnO_2 > α-MnO_2 > β-MnO_2.

[MnO_6] octahedra is thought as fundamental building unit in manganese oxides, which share two opposite edges to form a single octahedral chain, and two single chains further share two other adjacent edges from each octahedron to build a double chain (Meng *et al.*, 2014). Manganese oxides have diverse structures, depending on the connectivity between the [MnO_6] units via sharing corners or edges. The most common one is layered material δ-MnO_2, which has MnO_6-shared edges in each layer with cations such as Li^+, Na^+, and K^+ and other alkaline metals and water molecules occupying the space between the layers. One dimensional MnO_2 has tunnel structure, which would change along with the tunnel sizes. For instance, α-MnO_2 (2 × 2), β-MnO_2 (1 × 1), γ-MnO_2 (1 × 1 and 1 × 2) all belong to MnO_2 with tunnel structure (Huang *et al.*, 2010; Meng *et al.*, 2014).

Catalytic Oxidation for Formaldehyde

The catalytic activity of MnO_2 with different crystal structures over formaldehyde is shown in Fig. 2. In Fig. 2(a), all the MnO_2 can oxidize formaldehyde into CO_2 completely at 300°C, but different crystal forms show different performances. Complete conversions of HCHO over γ-MnO_2 and δ-MnO_2 were achieved at about 160°C, while that of α-MnO_2 and β-MnO_2 were both close to 300°C. To further explore the differences in activity of the γ-MnO_2 and δ-MnO_2, the top 2 activity catalysts, we have refined the temperature range of the two reactions in Fig. 2(b). Taking T_{90} as a starting point, every 5°C set as a temperature point, staying 20 min at each point to achieve completely decompose of formaldehyde, until the end of reaction.

The temperature of 10% (T_{10}), 50% (T_{50}), and 90% (T_{90}) CO_2 generation over MnO_2 are summarized in Table 2. The T90 over α-MnO_2, β-MnO_2, γ-MnO_2 and δ-MnO_2 were 248, 232, 138°C and 150°C, respectively, and the order of catalytic performance is: γ-MnO_2 > δ-MnO_2 > β-MnO_2 > α-MnO_2. Obviously, catalytic performance of γ-MnO_2 is the best among all these four kinds of catalysts.

Reducibility of Catalysts

Fig. 3 represents the profiles of H_2-TPR, which are used to evaluate the reducibility of the four samples. The final reduction products of MnO_2 could be MnO with Mn_2O_3 and Mn_3O_4 as intermediates (Jia *et al.*, 2016). As for α-MnO_2, two reduction peaks were observed at 280 and 328°C. The reduction peaks of δ-MnO_2 were similar to that of α-MnO_2 at 299 and 324°C, respectively. According to the literature, the lower temperature peak might be associated with the reduction of MnO_2 to Mn_3O_4, whereas the higher reduction peak should be attributed to the reduction of Mn_3O_4 to MnO (Liang *et al.*, 2008). The TPR profiles of β-MnO_2 and γ-MnO_2 were different from that of the α- and δ-MnO_2. Two reduction peaks were showed at 342 and 360°C for β-MnO_2, but the distribution of this two peaks was unclear, which might be related to the reduction of MnO_2 to MnO with Mn_2O_3 and Mn_3O_4 as intermediate (Xiang and Xie, 2001). There are three reduction peaks in γ-MnO_2 observed at 239, 263, and 343°C, respectively. However, the low

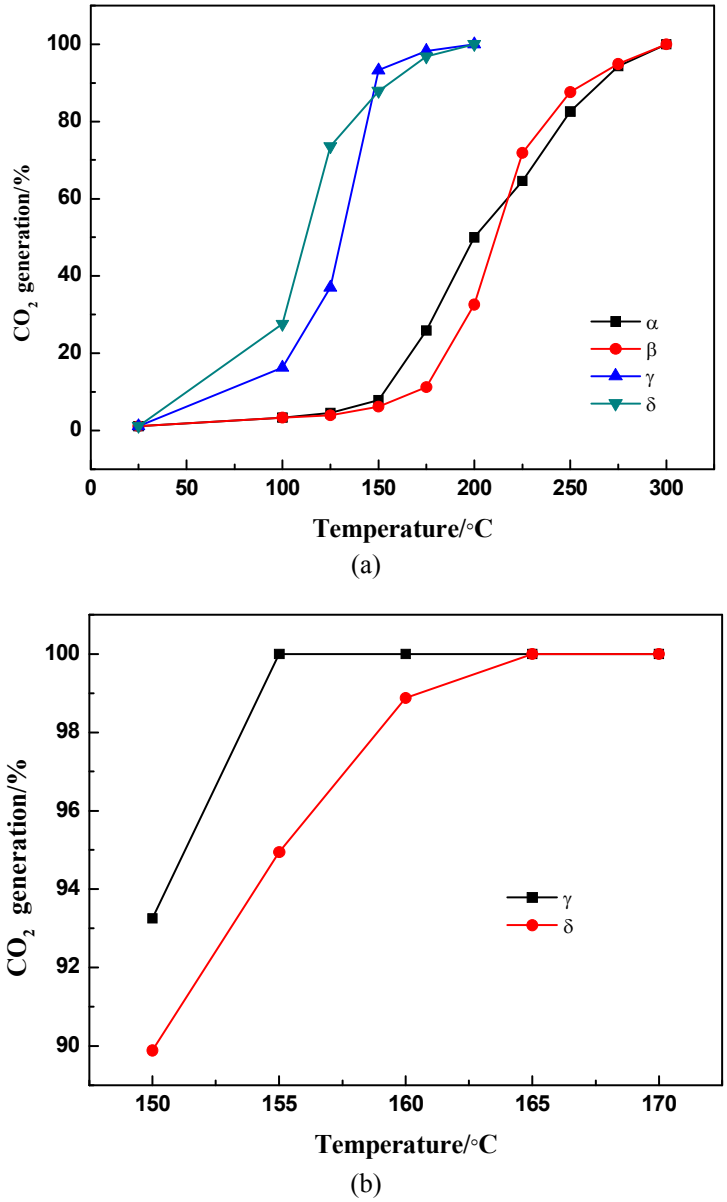

Fig. 2. The formation rates of CO_2 over four crystal forms of MnO_2 catalyst (a) and the top 2 activity catalysts (b).

Table 2. Catalytic activity of MnO_2 for formaldehyde oxidation.

Catalyst	CO_2 generation temperature/°C		
	T_{10}	T_{50}	T_{90}
α-MnO_2	120	200	248
β-MnO_2	180	218	232
γ-MnO_2	87	120	138
δ-MnO_2	82	118	150

temperature range is formed by the overlap of two peaks, which correspond to reduction of MnO_2 to Mn_2O_3/Mn_3O_4 and Mn_3O_4 to MnO.

The reducibility of catalyst improves along with the decrease of reduction temperature (Jia *et al.*, 2016). From the results of TPR, it is observed that γ-MnO_2 has the optimal reduction performance since it shows the reduction peak at the lowest temperature. Thus, the order of reduction is γ-MnO_2 >α-MnO_2 >δ-MnO_2 >β-MnO_2. This indicates that except β-MnO_2, there may exist relatively abundant loosely coupled surface oxygen species in other three catalysts (Jia *et al.*, 2016). Among the four samples, γ-MnO_2 is proven to possess the most mobile oxygen species.

NH_3-TPD

NH_3-TPD was used to identify the acidity of the catalysts. The quantities of acidic sites were estimated by integration of the area under the NH_3-TPD curve (Jia *et al.*, 2016) and the results are summarized in Table 3 and Fig. 4. The position of the peak can reveal the binding energy between acid sites and NH_3 molecule. Though α-MnO_2 contains the largest amount of acid sites, γ-MnO_2 contains much less acid sites than α-MnO_2, the desorption peaks at high temperature area of γ-MnO_2 appeared at 420 ºC which is higher than that of

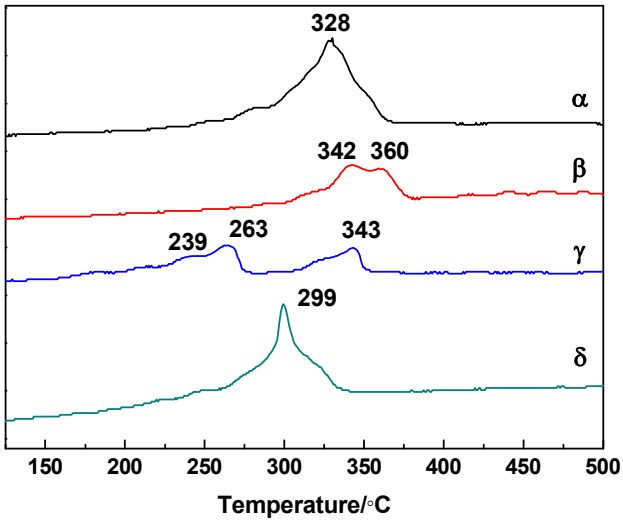

Fig. 3. H_2-TPR profiles of manganese oxides with different crystalline structures.

Table 3. The apparent activation energy of the catalytic oxidation of formaldehyde and the amounts of desorbed NH_3 over four crystal forms of MnO_2.

Catalyst	E_a (kJ mol^{-1})	Total acidity (μmol g^{-1})
α-MnO_2	0.79	208.44
β-MnO_2	1.74	37.95
γ-MnO_2	0.66	65.85
δ-MnO_2	0.60	45.52

α-MnO_2. For β- and δ-MnO_2 three desorption peaks were observed, which were slightly lower than those of γ-MnO_2. The binding energy of acid sites and NH_3 molecule will increase along with the temperature rise, indicating that γ-MnO_2 might possess the strongest acid sites of all. Besides, the exposed crystals of metal compound catalysts have significant effects on the catalytic activities. The crystal planes differ not only from the surface atom densities but also in the potential chemical reactions, hence resulting in the different surface energies.

XPS Analysis

To further confirm the oxidation state of the surface elements of the catalyst, the X-ray photoelectron spectrum analysis was carried out with the peaks associated with Mn 3s and O1s. Fig. 5(a) reveals energy spectrum of Mn 3s region. The average oxidation state (AOS) of Mn was estimated based on the following formula: $AOS = 8.956 - 1.126\Delta E_S$, where ΔE_S is the binding energy difference between the doublet Mn 3s peaks (Yang *et al.*, 2013). ΔE_S value is the basis for judging the oxidation state of the catalyst, and the ΔE_S value of MnO, Mn_2O_3 and MnO_2 are 6.0, 5.5 and 4.7 eV, respectively (Liu *et al.*, 2016). It shows that the range of ΔE_S value over four kinds of manganese oxides is 4.80–5.2eV, which indicates Mn^{4+} is not the only one valence for Mn element. The ΔE_S value of α-MnO_2 is 5.128, while the ΔE_S value of β-MnO_2, γ-MnO_2 and δ-MnO_2 are 4.81, 4.83 and 4.80, respectively. This data demonstrates the valence of α-MnO_2 is in favor of +3 oxidation state, and the valence of other three types of catalysts tends to +4 oxidation state. On the basis of results, AOS decreases in the order of δ-MnO_2 (3.55) > β-MnO_2 (3.53) > γ-MnO_2 (3.52) > α-MnO_2 (3.18), which suggests that the part of Mn^{4+} in δ-MnO_2 is the highest. It was reported that high Mn^{4+} concentration is advantageous to the catalytic combustion of hydrocarbons (Machocki *et al.*, 2004; Wu *et al.*, 2013). Comparison of Mn^{4+} ion concentration of catalysts, β-MnO_2 should have the best catalytic activity of all, but this does not match the experimental results. Obviously, γ-MnO_2 possesses better catalytic activity, and this might be attributed to its high specific surface area, which was conducive to the adsorption and diffusion of formaldehyde gas.

The O1s spectrum is often used to determine the types of surface oxygen species on the oxide. There are three obvious peaks in Fig. 5(b), which correspond to surface oxygen (O_α), lattice oxygen (O_β), and surface adsorbed water molecules ($O_{\alpha'}$), respectively. For all of samples, the binding energy of 529.7–530.1 eV is attributed to lattice oxygen (like O^{2-}); the binding energy of 531.3–531.8 eV is attributed to surface oxygen (like O_2^{2-}, O^-, OH^-, CO_3^{2-}); And the binding energy of 532.4–533.2 eV is attributed to surface adsorbed water molecules (Dai *et al.*, 2011). It can be seen from Table 4 that γ-MnO_2 has the highest proportion of O_α/O_β, demonstrating γ-MnO_2 contains the most abundant surface adsorbed oxygen (O^-, OH^-). This result suggests γ-MnO_2 owns the highest density of oxygen vacancies, because oxygen molecules are usually absorbed at the oxygen vacancies of an oxide material (Wang *et al.*, 2012).

Generally speaking, the higher oxidation state of manganese oxide, the more favorable to the catalytic oxidation process. But this is contrary to the results of Fig. 1, which shows that the oxidation state is not the only factor to determine the catalytic activity of manganese oxide. Combining with previous characterization results, γ-MnO_2 has large specific surface area, richest surface oxygen vacancies, open pore structure and abundant surface oxygen species with loose combination. All these characteristics provide more active sites for the formaldehyde gas, as well

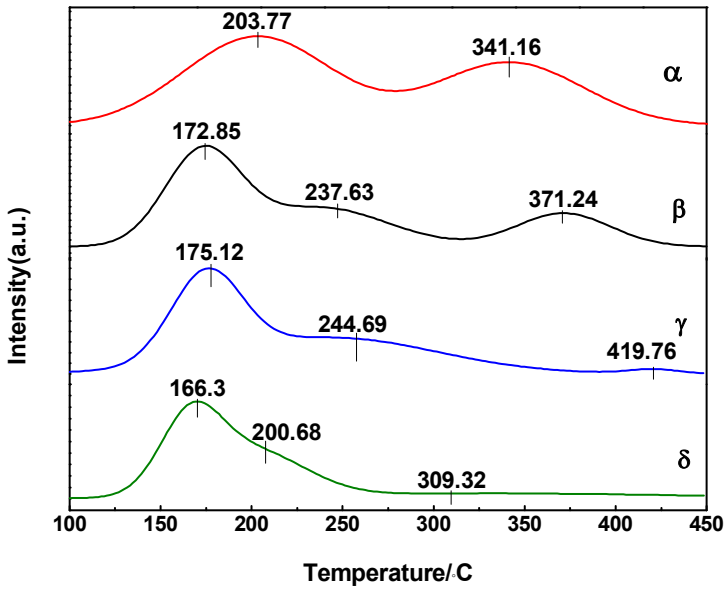

Fig. 4. NH_3-TPD curves of manganese oxides with different crystalline structures.

as accelerate the diffusion of O_2 and enhance the surface oxygen flow. For β-MnO_2, its lowest specific surface area and average pore diameter will restrict the internal diffusion rate of pollutants enormously, along with lacking acid sites, thus led to its weak catalytic capability. For α-MnO_2, the lowest Mn^{4+} concentration might be responsible for its worse oxidation activity. As for δ-MnO_2, despite its highest AOS and specific surface area, it cannot provide enough active sites, as well as the weak oxygen vacancies, consequently reducing its catalytic activity.

Calculation of E_a Value

Fig. 6 shows the Arrhenius plots for formaldehyde decomposition over the four MnO_2 catalysts. According to the slope of the curve, the apparent activation energy of oxidation of formaldehyde can be evaluated and summarized in Table 3. The apparent activation energy is 0.60 kJ mol^{-1} on δ-MnO_2, 0.66 kJ mol^{-1} on γ-MnO_2, 1.74 kJ mol^{-1} on β-MnO_2 and 0.79 kJ mol^{-1} on α-MnO_2. Among these, the apparent activation energy of δ-MnO_2 and γ-MnO_2 are nearly the same, which suggests that the surface of these two samples are easier to be activated at low temperature. Although the apparent activation energy of γ-MnO_2 is slightly higher than that of δ-MnO_2, γ-MnO_2 still has better catalytic activity for its abundant surface oxygen vacancies, which eliminates the tiny gap between the E_a value of these two catalysts. As we can see, the catalytic activity is not consistent with the changing trend of the activation energy as usual. Shi *et al.* (2012) had found the same phenomenon as we did, in which the best catalyst owned the highest E_a value among the three synthetic samples.

Reaction Mechanism of Formaldehyde Catalytic Oxidation

In previous study, Mars-Van Krevelen (MVK) mechanism has been explained for the catalytic oxidation of VOCs over metal oxides (Wu *et al.*, 2011; Huang *et al.*, 2015). The reaction procedure consists of two redox steps: firstly, the catalyst in the gas phase is oxidized by oxygen to form the surface oxygen species, including surface lattice oxygen; Then, VOCs molecules are oxidized by surface oxygen and reduction of the oxidized catalysts by hydrocarbon compounds. Especially for HCHO, its oxidation over metal oxide includes the reaction between HCHO and surface oxygen to form the intermediate formate (Eqs. (2) and (3)) , and the oxidation of formate to H_2O and CO_2 by surface oxygen at different sites, accompanied with the catalyst reduced (Eqs. (4) and (5)) (Sekine, 2002).

$$HCHO(g) + O(a) \rightarrow HCHOO(a) \quad (2)$$

$$HCHOO(a) \rightarrow HCOO(a) + H(a) \quad (3)$$

$$HCOO(a) \rightarrow H(a) + CO_2(g) \quad (4)$$

$$2H(a) + O(g) \rightarrow H_2O \quad (5)$$

where (g) and (a) refers to the gaseous and absorbed species, respectively. Thus, the catalytic oxidation of formaldehyde depends on many factors. In addition to the physical and chemical properties of the catalyst itself, the removal efficiency of formaldehyde is also closely related to the reduction and surface oxygen vacancies content of the catalysts.

Effect of H_2O and SO_2 over γ-MnO_2 Catalyst

Since H_2O is an integral part of the composition of the air, and SO_2 has become an assignable factor for the release of some chemical companies after desulfuration. It is necessary to discuss the influence of H_2O and SO_2 on the catalytic activity. In order to simulate the content of H_2O and SO_2 in air, we refer to the relevant knowledge and determine the concentration of H_2O and SO_2. As shown in Fig. 7, when 1% H_2O is added, the CO_2 generation of γ-MnO_2

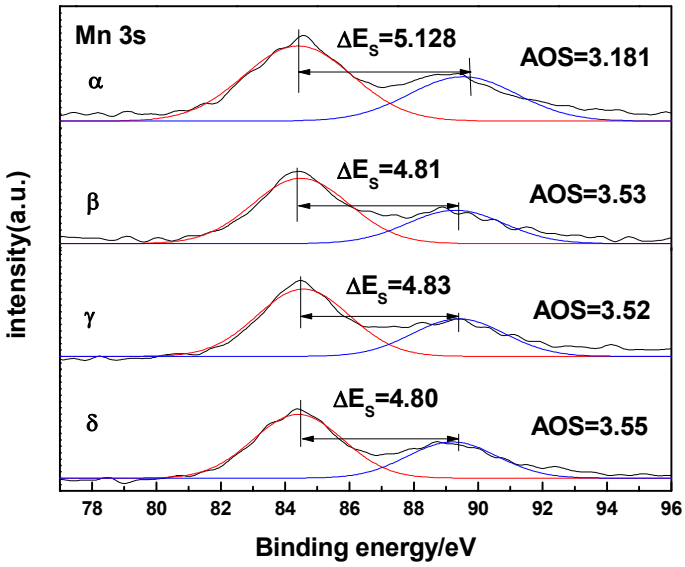

(a)

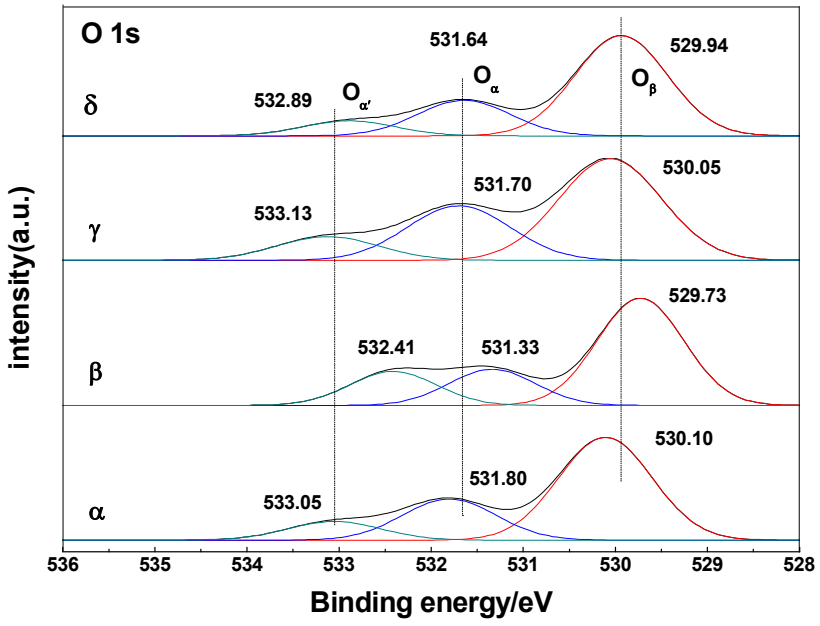

(b)

Fig. 5. XPS analysis of different crystal structure of MnO_2: Mn 3s (a), O 1s (b).

Table 4. XPS results of MnO_2.

Catalyst	Oxygen distribution/%			E_b (Mn 2p)/eV	
	O_β	O_α	O_α/O_β	Mn $2P_{1/2}$	Mn $2P_{3/2}$
α-MnO_2	63.28	25.25	0.39	653.9	642.2
β-MnO_2	50.50	20.36	0.40	653.9	642.2
γ-MnO_2	56.51	30.32	0.53	653.9	642.2
δ-MnO_2	66.49	23.57	0.35	653.9	642.2

stays steady at first, then rapidly falls to 65% and only recover to 80% after removing the H_2O. These results show that the inhibiting effect of H_2O on the catalytic activity is incomplete reversible. When 100 ppm of SO_2 is added, the CO_2 generation of γ-MnO_2 decreases from 100% to about 20%, and can not recover at all when SO_2 is off. This might be owing to the formation of sulfate ion under the presence of SO_2 and H_2O. When SO_2 and formaldehyde were led into the reactor, sulfate ion formed and adsorbed on the catalyst's surface, which will compete with pollutants for active sites and result in irreversible inactivation (Ao *et al.*, 2004a, b). The co-existence of SO_2 and H_2O in feed gas causes a rapid decline at the beginning of the reaction, and then decreases slowly from 34% to 12% and remain stable. After shutting off SO_2 and H_2O, the CO_2 generation increases only 10%. As simultaneous existence of SO_2 and H_2O, competitive adsorption of SO_2 and H_2O causes the deactivation of catalyst and shortens its life.

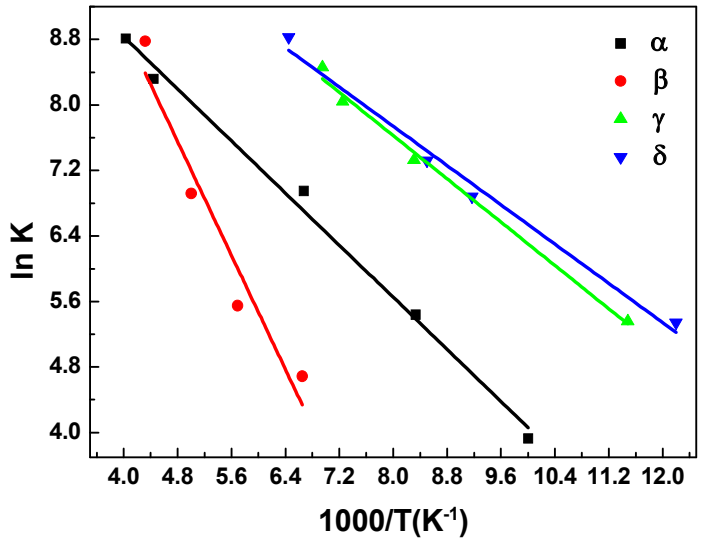

Fig. 6. Arrhenius plots for formaldehyde decomposition over α-, β-, γ- and δ-MnO_2.

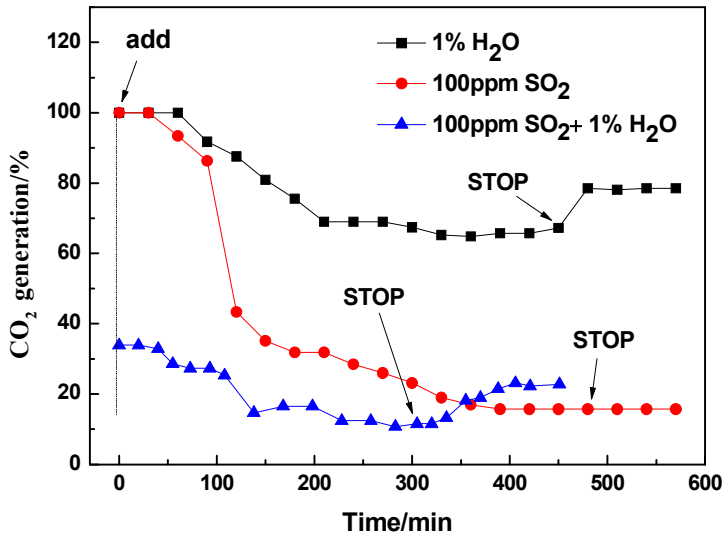

Fig. 7. Impact of H_2O and SO_2 over γ-MnO_2 catalyst.

CONCLUSIONS

Four different crystal forms of MnO_2 nanoparticles were prepared by hydrothermal method and were tested for the destruction and removal (DRE) of formaldehyde. The physicochemical properties of the catalysts were characterized by the XRD, BET, H_2-TPR, NH_3-TPD, and XPS techniques. Under the condition of formaldehyde concentration = 1400 ppm, and SV = 100000 mL g^{-1} h^{-1}, the active temperature window of γ-MnO_2 was 155°C, while the same conversions on α-MnO_2, β-MnO_2 and δ-MnO_2 were obtained at 275, 300 and 165°C, respectively. The apparent activation energies of the four forms of MnO_2 were in the range of 0.6–1.8 kJ mol^{-1}. According to the experimental result, the synthesized MnO_2 possessed almost 100% Mn^{4+} ion enriching on the surface. It can be concluded that the surface concentration of Mn^{4+} ion is significant to its high catalytic activity for the catalytic oxidation of formaldehyde. The TPR and TPD results suggest γ-MnO_2 possess large specific surface area, strong binding sites and loosely combined surface oxygen, which will be propitious to the adsorption and diffusion of the reactants. Besides, the proportion of O_α/O_β for γ-MnO_2 is 0.53, which is apparently higher than those of the other three catalysts. Indicating γ-MnO_2 owns the most abundant oxygen vacancies, which is ascribed as the most critical factor for the catalytic oxidation of formaldehyde in this novel.

ACKNOWLEDGEMENTS

This study was funded by the Program of National Science Foundation of China (No. 41202021), Guangdong Provincial Key Laboratory of Mineral Physics and Materials (No. GLMPM-004), and the Fundamental Research Funds for the Central Universities (No. 2014HGQC0139). The authors appreciate the editor and reviewers for their suggestion and comments.

REFERENCES

Ao, C.H., Lee, S.C., Yu, J.Z. and Xu, J.H. (2004a). Photodegradation of formaldehyde by photocatalyst TiO_2: Effects on the presences of NO, SO_2 and VOCs. *Appl. Catal., B* 54: 41–50.

Ao, C.H., Lee, S.C., Zou, S.C. and Mak, C.L. (2004b). Inhibition effect of SO_2 on NO_x and VOCs during the photodegradation of synchronous indoor air pollutants at parts per billion (ppb) level by TiO_2. *Appl. Catal., B* 49: 187–193.

Atkinson, R. and Arey, J. (2003a). Atmospheric degradation of volatile organic compounds. *Chem. Rev.* 103: 4605–4638.

Atkinson, R. and Arey, J. (2003b). Gas-phase tropospheric chemistry of biogenic volatile organic compounds: A review. *Atmos. Environ.* 37: 197–219.

Bai, B., Qiao, Q., Li, J. and Hao, J. (2016). Progress in research on catalysts for catalytic oxidation of formaldehyde. *Chin. J. Catal.* 37: 102–122.

Chen, D., Qu, Z., Sun, Y. and Wang, Y. (2014). Adsorption-desorption behavior of gaseous formaldehyde on different porous Al_2O_3 materials. *Colloids Surf., A* 441: 433–440.

Chen, D., Qu, Z., Lv, Y., Lu, X., Chen, W. and Gao, X. (2015). Effect of oxygen pretreatment on the surface catalytic oxidation of HCHO on Ag/MCM-41 catalysts. *J. Mol. Catal. A: Chem.* 404–405: 98–105.

Collins, J.J., Ness, R., Tyl, R.W., Krivanek, N., Esmen, N.A. and Hall, T.A. (2001). A Review of Adverse Pregnancy Outcomes and Formaldehyde Exposure in Human and Animal Studies. *Regul. Toxicol. Pharm.* 34: 17–34.

Dai, Y., Wang, X., Li, D. and Dai, Q. (2011). Catalytic combustion of chlorobenzene over Mn-Ce-La-O mixed oxide catalysts. *J. Hazard. Mater.* 188: 132–139.

Ewlad-Ahmed, A.M., Morris, M.A., Patwardhan, S.V. and Gibson, L.T. (2012). Removal of formaldehyde from air using functionalized silica supports. *Environ. Sci. Technol.* 46: 13354–13360.

Hosseini, S.R., Raoof, J., Ghasemi, S. and Gholami, Z. (2016). Pd-Cu/poly(o-Anisidine) nanocomposite as an efficient catalyst for formaldehyde oxidation. *Mater. Res. Bull.* 80: 107–119.

Huang, H., Chen, C., Xu, L., Genuino, H., Garcia-Martinez, J., Garces, H.F., Jin, L., Kithongo, C.K. and Suib, S.L. (2010). Single-step synthesis of manganese oxide octahedral molecular sieves with large pore sizes. *Chem. Commun.* 46: 5945.

Huang, H., Xu, Y., Feng, Q. and Leung, D.Y.C. (2015). Low temperature catalytic oxidation of volatile organic compounds: A review. *Catal. Sci. Technol.* 5: 2649–2669.

Jia, J., Zhang, P. and Chen, L. (2016). Catalytic decomposition of gaseous ozone over manganese dioxides with different crystal structures. *Appl. Catal., B* 189: 210–218.

Jin, L., Chen, C., Crisostomo, V.M.B., Xu, L., Son, Y. and Suib, S.L. (2009). γ-MnO_2 octahedral molecular sieve: Preparation, characterization, and catalytic activity in the atmospheric oxidation of toluene. *Appl. Catal., A* 355: 169–175.

Kim, S. (2009). Environment-friendly adhesives for surface bonding of wood-based flooring using natural tannin to reduce formaldehyde and TVOC emission. *Bioresour. Technol.* 100: 744–748.

Kosuge, K., Kubo, S., Kikukawa, N. and Takemori, M. (2007). Effect of pore structure in mesoporous silicas on VOC dynamic adsorption/desorption performance. *Langmuir* 23: 3095–3102.

Liang, S., Teng, F., Bulgan, G., Zong, R. and Zhu, Y. (2008). Effect of phase structure of MnO_2 nanorod catalyst on the activity for CO oxidation. *J. Phys. Chem. C* 112: 5307–5315.

Liang, X., Liu, P., He, H., Wei, G., Chen, T., Tan, W., Tan, F., Zhu, J. and Zhu, R. (2016). The variation of cationic microstructure in Mn-doped spinel ferrite during calcination and its effect on formaldehyde catalytic oxidation. *J. Hazard. Mater.* 306: 305–312.

Liu, H., Chen, T., Chen, D., Chang, D. and Frost, R.L. (2013). The development of a new method for the determination of concentrations of carbonaceous gases using a non-dispersive infrared sensor. *Fuel* 104: 749–751.

Liu, P., He, H., Wei, G., Liang, X., Qi, F., Tan, F., Tan, W., Zhu, J. and Zhu, R. (2016). Effect of Mn substitution on the promoted formaldehyde oxidation over spinel ferrite: Catalyst characterization, performance and reaction mechanism. *Appl. Catal., B* 182: 476–484.

Ma, C., Li, X. and Zhu, T. (2011). Removal of low-concentration formaldehyde in air by adsorption on activated carbon modified by hexamethylene diamine. *Carbon* 49: 2873–2875.

Machocki, A., Ioannides, T., Stasinska, B., Gac, W., Avgouropoulos, G., Delimaris, D., Grzegorczyk, W. and Pasieczna, S. (2004). Manganese-lanthanum oxides modified with silver for the catalytic combustion of methane. *J. Catal.* 227: 282–296.

Meng, Y., Song, W., Huang, H., Ren, Z., Chen, S. and Suib, S.L. (2014). Structure-property relationship of bifunctional MnO_2 nanostructures: Highly efficient, ultra-stable electrochemical water oxidation and oxygen reduction reaction catalysts identified in alkaline media. *J. Am. Chem. Soc.* 136: 11452–11464.

Sekine, Y. (2002). Oxidative decomposition of formaldehyde by metal oxides at room temperature. *Atmos. Environ.* 36: 5543–5547.

Shi, F., Wang, F., Dai, H., Dai, J., Deng, J., Liu, Y., Bai, G., Ji, K. and Au, C.T. (2012). Rod-, flower-, and dumbbell-like MnO_2: Highly active catalysts for the combustion of toluene. *Appl. Catal., A* 433–434: 206–213.

Silbergeld, E.K. and Patrick, T.E. (2005). Environmental exposures, toxicologic mechanisms, and adverse pregnancy outcomes. *Am. J. Obstet. Gynecol.* 192: 11–21.

Spivey, J.J. (1987). Complete catalytic oxidation of volatile organics. *Ind. Eng. Chem. Res.* 26: 2165–2180.

Tang, X., Bai, Y., Duong, A., Smith, M. T., Li, L. and Zhang, L. (2009). Formaldehyde in China: Production, consumption, exposure levels, and health effects. *Environ. Int.* 35: 1210–1224.

Wang, F., Dai, H., Deng, J., Bai, G., Ji, K. and Liu, Y. (2012). Manganese oxides with rod-, wire-, tube-, and

flower-like morphologies: highly effective catalysts for the removal of toluene. *Environ. Sci. Technol.* 46: 4034–4041.

Wang, R. and Li, J. (2010). Effects of precursor and sulfation on OMS-2 catalyst for oxidation of ethanol and acetaldehyde at low temperatures. *Environ. Sci. Technol.* 44: 4282–4287.

Wang, X., Gong, M., Guo, J., Qu, Y., Yin, H., Liu, Y. and Li, J. (2015). Effects oF Mn-loading on activated carbon treated by HNO_3 for SO_2 removal. *Fresenius Environ. Bull.* 24: 1291–1301.

Wu, H., Wang, L., Zhang, J., Shen, Z. and Zhao, J. (2011). Catalytic oxidation of benzene, toluene and p-xylene over colloidal gold supported on zinc oxide catalyst. *Catal. Commun*. 12: 859–865.

Wu, L., Zhang, L., Meng, T., Yu, F., Chen, J. and Ma, J. (2015b). Facile synthesis of 3D amino-functional graphene-sponge composites decorated by graphene nanodots with enhanced removal of indoor formaldehyde. *Aerosol Air Qual. Res*. 15: 1028–1034.

Wu, X., Huang, W., Zhang, Y., Zheng, C., Jiang, X., Gao, X. and Cen, K. (2015a). Characteristics and uncertainty of industrial VOCs emissions in China. *Aerosol Air Qual. Res*. 15: 1045–1058.

Wu, Y., Lu, Y., Song, C., Ma, Z., Xing, S. and Gao, Y. (2013). A novel redox-precipitation method for the preparation of α-MnO_2 with a high surface Mn^{4+} concentration and its activity toward complete catalytic oxidation of o-xylene. *Catal. Today* 201: 32–39.

Xiang, W. and Xie, Y.C. (2001). The promotion effects of Ba on manganese oxide for CH_4 deep oxidation. *Catal. Lett.* 72: 51–57.

Yang, Y., Huang, J., Wang, S., Deng, S., Wang, B. and Yu, G. (2013). Catalytic removal of gaseous unintentional POPs on manganese oxide octahedral molecular sieves. *Appl. Catal., B* 142–143: 567–568.

Yu, B., He, W., Li, N., Yang, F. and Ji, J. (2016). Thermal catalytic oxidation performance study of SWTCO system for the degradation of indoor formaldehyde: Kinetics and feasibility analysis. *Build. Environ.*108: 183–193.

Yu, K., Lee, W. G. and Lin, G. (2015). Removal of low-concentration formaldehyde by a fiber optic illuminated honeycomb monolith photocatalytic reactor. *Aerosol Air Qual. Res*. 15: 1008–1016.

Yuan, J.K., Laubernds, K., Zhang, Q.H. and Suib, S.L. (2003). Self-assembly of microporous manganese oxide octahedral molecular sieve hexagonal flakes into mesoporous hollow nanospheres. *J. Am. Chem. Soc.* 125: 4966–4967.

Zeng, W. and Bai, H. (2016). Adsorption/desorption behaviors of acetone over Micro-/Mesoporous SBA-16 silicas prepared from rice husk agricultural waste. *Aerosol Air Qual. Res*. 16: 2267–2277.

Zhou, L., Zhang, J., He, J., Hu, Y. and Tian, H. (2011). Control over the morphology and structure of manganese oxide by tuning reaction conditions and catalytic performance for formaldehyde oxidation. *Mater. Res. Bull.* 46: 1714–1722.

Received for review, January 7, 2017
Revised, February 28, 2017
Accepted, March 3, 2017